HHS Public Access

Author manuscript

*Neurobiol Dis*. Author manuscript; available in PMC 2024 May 01.

Published in final edited form as:

*Neurobiol Dis*. 2024 May ; 194: 106470. doi:10.1016/j.nbd.2024.106470.

# Altered neurological and neurobehavioral phenotypes in a mouse model of the recurrent *KCNB1*-p.R306C voltage-sensor variant

**Seok Kyu Kang**[a,b,1], **Nicole A. Hawkins**[a,1], **Christopher H. Thompson**[a], **Erin M. Baker**[a], **Dennis M. Echevarria-Cooper**[a,b], **Levi Barse**[a], **Tyler Thenstedt**[a], **Conor J. Dixon**[a], **Nathan Speakes**[a], **Alfred L. George Jr**[a,b], **Jennifer A. Kearney**[a,b,*]

[a]Department of Pharmacology, Feinberg School of Medicine, Northwestern University, Chicago, IL 60611, USA

[b]Northwestern University Interdepartmental Neuroscience Program, Northwestern University, Chicago, IL 60611, USA

## Abstract

Pathogenic variants in *KCNB1* are associated with a neurodevelopmental disorder spectrum that includes global developmental delays, cognitive impairment, abnormal electroencephalogram (EEG) patterns, and epilepsy with variable age of onset and severity. Additionally, there are prominent behavioral disturbances, including hyperactivity, aggression, and features of autism spectrum disorder. The most frequently identified recurrent variant is *KCNB1*-p.R306C, a missense variant located within the S4 voltage-sensing transmembrane domain. Individuals with the R306C variant exhibit mild to severe developmental delays, behavioral disorders, and a diverse spectrum of seizures. Previous in vitro characterization of R306C described altered sensitivity and cooperativity of the voltage sensor and impaired capacity for repetitive firing of neurons. Existing *Kcnb1* mouse models include dominant negative missense variants, as well as knockout and frameshifts alleles. While all models recapitulate key features of *KCNB1* encephalopathy, mice with dominant negative alleles were more severely affected. In contrast to existing loss-of-function and dominant-negative variants, *KCNB1*-p.R306C does not affect channel expression, but



*Corresponding author at: Northwestern University, Feinberg School of Medicine, 320 East Superior Street, Searle 8-510, Chicago, IL 60611, USA. jennifer.kearney@northwestern.edu (J.A. Kearney).

[1]Contributed equally to this work.

CrediT authorship contribution statement

**Seok Kyu Kang:** Conceptualization, Methodology, Formal analysis, Investigation, Writing - Original Draft, Writing - Review & Editing, Visualization. **Nicole A. Hawkins:** Conceptualization, Methodology, Formal analysis, Investigation, Writing - Original Draft, Writing - Review & Editing, Visualization, Project administration. **Christopher H. Thompson:** Conceptualization, Formal analysis, Investigation, Writing -Review & Editing, Visualization. **Erin M. Baker:** Investigation, Formal analysis, Writing - Review & Editing. **Dennis-Echevarria-Cooper:** Investigation, Formal analysis, Writing - Review & Editing. **Levi Barse**: Investigation, Writing - Review & Editing; **Tyler Thenstedt**: Investigation; Writing - Review & Editing, Visualization; **Conor J. Dixon:** Investigation, Formal analysis, Writing - Review & Editing. **Nathan Speakes:** Investigation, Formal analysis, Writing - Review & Editing. **Alfred** L. **George, Jr.**: Conceptualization, Writing - Review & Editing, Funding acquisition; **Jennifer A. Kearney:** Conceptualization, Formal analysis, Investigation, Writing - Review & Editing, Visualization, Project administration, Funding acquisition.

Supplementary data to this article can be found online at https://doi.org/10.1016/j.nbd.2024.106470.

Declaration of competing interest

The authors declare no competing interests related to this study.

rather affects voltage-sensing. Thus, modeling R306C in mice provides a novel opportunity to explore impacts of a voltage-sensing mutation in *Kcnb1*. Using CRISPR/Cas9 genome editing, we generated the *Kcnb1*$^{R306C}$ mouse model and characterized the molecular and phenotypic effects. Consistent with the in vitro studies, neurons from *Kcnb1*$^{R306C}$ mice showed altered excitability. Heterozygous and homozygous R306C mice exhibited hyperactivity, altered susceptibility to chemoconvulsant-induced seizures, and frequent, long runs of slow spike wave discharges on EEG, reminiscent of the slow spike and wave activity characteristic of Lennox Gastaut syndrome. This novel model of channel dysfunction in *Kcnb1* provides an additional, valuable tool to study *KCNB1* encephalopathies. Furthermore, this allelic series of *Kcnb1* mouse models will provide a unique platform to evaluate targeted therapies.

**Keywords**

Epilepsy; Encephalopathy; Developmental disorder; Autism spectrum disorder; $K_V$2.1; Voltage-gated potassium channels; Voltage-gated ion channels

## 1. Introduction

Disease phenotyping in animal models is an important step for understanding many aspects of human physiological and pathological processes. This is especially true for neurological diseases that are often rare and complex, because the manifestation of disease phenotypes involves advanced dimensions of human biology such as the collective environment (i.e. neural circuitry) and time (i.e. neurodevelopment), which cannot be adequately addressed in non-animal experimental systems like cell culture or computational methods (Chesselet and Carmichael, 2012). CRISPR/Cas9 genome editing technology has enabled faster and more accurate recapitulation of human diseases in mice, and thus accelerated construction of genotype-phenotype correlations for rare diseases with genetic basis (Aida et al., 2014; Platt et al., 2014).

*KCNB1* encephalopathy is a rare autosomal dominant disorder caused by pathogenic variants in the *KCNB1* gene that most often arise de novo in the affected child. Individuals with *KCNB1* encephalopathy present with global developmental delay in infancy or early childhood accompanied by features of autism spectrum disorder, abnormal EEG patterns, and development of epilepsy in most children, although epilepsy severity and treatment response are variable (Bar et al., 2020a; Bar et al., 2020b; de Kovel et al., 2017; Kang et al., 2019; Saitsu et al., 2015; Scheffer and Liao, 2020; Thiffault et al., 2015; Torkamani et al., 2014). *KCNB1,* encoding the $K_V$2.1 voltage-gated potassium channel alpha subunit, is a critical contributor to neuronal repolarization and homeostasis (Murakoshi and Trimmer, 1999). The majority of *KCNB1* variants studied thus far in heterologous cells and cultured neurons have been shown to confer an ultimate outcome of loss-of-function (LoF) that prevents the channel from conducting $K^+$ ions across the plasma membrane (Kang et al., 2019; Saitsu et al., 2015; Thiffault et al., 2015). Although the ultimate outcome is largely LoF, there are several classes of underlying mechanisms that lead to diminished channel function, including defective $K_V$2.1 synthesis, trafficking, or function. Targeted therapies tailored to the specific mechanism can improve patient out-comes (Haq et al., 2022; Tian

et al., 2022), highlighting the importance of representing these different mechanisms in preclinical animal models. Variants modeled in mice to date have focused on those that affect $K_V$2.1 expression, including *Kcnb1*$^{G379R}$, *Kcnb1*$^{R312H}$ and *Kcnb1* null and frameshift alleles (Bortolami et al., 2022; Hawkins et al., 2021; Speca et al., 2014). *KCNB1*-p.G379R exhibited a dominant-negative LoF phenotype with altered ion-selectivity in CHO-K1 cells (Torkamani et al., 2014), and recapitulated dominant-negative cellular phenotypes, epilepsy, background EEG abnormalities and neurobehavioral symptoms in mice (Hawkins et al., 2021). *KCNB1*-p.R312H exhibited a LoF phenotype with deficient cell surface expression in CHO-K1 cells, and diminished $K_V$2.1 protein and seizures in knock-in mice (Bortolami et al., 2022; Kang et al., 2019).

*KCNB1*-p.R306C is one of the most recurrent variants and represents another major class of channel dysfunction, diminished function due to altered voltage-sensing (Kang et al., 2019). At least six cases with *KCNB1*-p.R306C have been described in the literature and severity of the associated phenotypes ranges from mild developmental disability with absence epilepsy to severe developmental disability with intractable epilepsy that includes multiple seizure types (Bar et al., 2020a; de Kovel et al., 2017; Kang et al., 2019; Saitsu et al., 2015). Arginine 306 is one of the positively charged residues in the S4 transmembrane domain that is critical for voltage-sensor function of the $K_V$2.1 channel (Catacuzzeno and Franciolini, 2022). Functional studies of the R306C variant in heterologous expression systems showed normal cell surface expression, but loss of $K_V$2.1 channel current and shifts in voltage-dependence of activation (Kang et al., 2019; Saitsu et al., 2015; Fernández-Mariño et al., 2023). Consistent with this, transient overexpression in primary cultured cortical pyramidal neurons resulted in lower sensitivity and cooperativity of the voltage sensor and severely impaired capacity for repetitive firing (Saitsu et al., 2015). To model $K_V$2.1 voltage-sensor dysfunction in vivo, we generated and characterized a novel *Kcnb1*$^{R306C}$ mouse line using CRISPR/Cas9 genome editing (Platt et al., 2014). We evaluated the effects of heterozygosity and homozygosity for the R306C variant on $K_V$2.1 expression and localization in cultured neurons, as well as seizure susceptibility, EEG, and locomotor activity in behaving mice. Although expression and localization of $K_V$2.1 was unaffected, *Kcnb1*$^{R306C}$ mice displayed altered hippocampal pyramidal neuron excitability, altered susceptibility to induced seizures by flurothyl and kainic acid (KA), significant epileptiform and interictal EEG abnormalities, and behavioral hyperactivity. Thus, *Kcnb1*$^{R306C}$ mice recapitulate key features of *KCNB1* encephalopathy and will be a useful platform for studying disease mechanisms, probing variable expressivity, and evaluating potential therapies.

## 2. Methods

### 2.1. Mice

Gene editing was performed in fertilized C57BL/6J embryos via electroporation of CRISPR components. The Cas9 protein was complexed with a CRISPR guide RNA (gRNA), which generated DNA double strand break in exon 2 of the *Kcnb1* gene (gRNA sequence: 5’ GGGCCAACTTCAGGATGCGC 3’). A single-stranded donor oligonucleotide (ssODN) was included in the reaction to introduce the R306C point mutation via homology dependent repair (HDR)

The ssODN sequence is as follows: 5'CTGCGCAGCGTGAAGCCCAAGGACTGCA-GACCGGTGGAGTGGCGGGCCAACTTCAGGAT**GCa**CAG***aAT***GCGCAT GATGCGGAAGATCTGGACCACACGGCGCACATTCTGGAACTGCAGC 3′. This was designed as an antisense sequence, complementary to the sense (coding) strand. Highlighted in bold is a change in the coding sequence from CGC➔tGC, resulting in the *Kcnb1* R306C point mutation upon ssODN mediated HDR. Highlighted in bold italics is a silent mutation changing coding of the Ile from ATC-ATt which disrupts the protospacer adjacent motif (PAM, -NGG) site preventing re-cutting of the site once ssODN mediated HDR occurs.

For the CRISPR components we used the AltR-Cas9 system (Integrated DNA Technologies, Inc. (IDT), Coralville, Iowa). Briefly, the gRNA was custom synthesized as crRNA and complexed with tracrRNA (IDT, 1070532) to form the gRNA complex. It was combined with HiFidelity Cas9 protein (IDT, 1081064) to form the ribonucleotide protein complex (RNP). The 120 nucleotide ssODN (IDT) was added to the reaction mixture after RNP formation, prior to electroporation. The final concentration of the electroporation mixture was 3 μM Cas9, 3 μM gRNA, 10 μM ssODN.

Potential founders were screened by PCR of genomic DNA with primers outside of the homology region for the repair oligo (Table 1). PCR products were cloned into pCR-TOPO (ThermoFisher) and Sanger sequenced. The mosaic R306C founder was backcrossed to C57BL/6J mice (Jackson Labs, #000664, Bar Harbor, ME) to generate N1 offspring. The N1 offspring were genotyped by Sanger sequencing to confirm transmission of the R306C editing event and absence of off-target events at predicted sites with <3 mismatches. N1 males with the confirmed on-target event and without predicted off-target events were bred with C57BL/6J females to establish the line $Kcnb1^{em3Kea}$ (MGI: 675522; MMRRC 071286-UCD), which has been maintained as an isogenic strain on C57BL/6J by continual backcrossing of $Kcnb1^{R306C}$ heterozygous mice (abbreviated $Kcnb1^{C/+}$) with inbred C57BL/6J mice. Mice were bred for at least 3 generations prior to experiments. For experiments, male and female $Kcnb1^{C/+}$ mice were intercrossed to generate $Kcnb1^{+/+}$ wildtype (WT), heterozygous $Kcnb1^{C/+}$ (C/+), and homozygous $Kcnb1^{C/C}$ (C/C) mice.

Mice were maintained in a Specific Pathogen Free (SPF) barrier facility with a 14-h light/10-h dark cycle and access to food and water ad libitum. Both female and male mice were used for all experiments. All animal care and experimental procedures were approved by the Northwestern University Animal Care and Use Committees in accordance with the National Institutes of Health Guide for the Care and Use of Laboratory Animals. The principles outlined in the ARRIVE (Animal Research: Reporting of in vivo Experiments) guideline were considered when planning experiments (Percie du Sert et al., 2020).

## 2.2. Genotyping

Mice were genotyped by PCR of genomic DNA isolated from tail biopsies, using a restriction fragment length polymorphism (RFLP) assay. Genomic DNA was amplified using RFLP genotyping primers (Table 1), followed by restriction digest with *Bsm*I for at least 15 min at 65 °C. Digestion resulted in 402 bp and 253 bp products for the mutant allele and 655 bp for the WT allele.

### 2.3. Transcript analysis

Forebrain isolated from male and female WT, *Kcnb1*$^{C/+}$ and *Kcnb1*$^{C/C}$ mice at postnatal days 58–83 (P58–83) was used for total RNA extraction using TRIZol reagent according to the manufacturer's instructions (Invitrogen). First strand cDNA was synthesized using 4 μg of RNA using oligo(dt) primer and Superscript IV according to the manufacturer's instructions (Life Technologies). First strand cDNA samples were diluted 1:10 and 5 μL was used as template with ddPCR Supermix for Probes (No dUTP) (Bio-Rad) and TaqMan Gene Expression Assays (Life Technologies) for mouse *Kcnb1* (FAM-MGB-Mm00492791_m1) and *Tbp* (normalization control; VIC-MGB-Mm00446971_m1). Reactions were partitioned into a QX200 droplet generator (Bio-Rad) and then amplified using PCR conditions: 95 °C for 10 min, 44 cycles of 95 °C for 30 s and 60 °C for 1 min (ramp rate of 2 °C/s) with a final inactivation step of 98 °C for 5 min. Following amplification, droplets were analyzed with a QX200 droplet reader and QuantaSoft vl.6.6 software (Bio-Rad). Relative transcript levels were expressed as a ratio of *Kcnb1* to *Tbp* with WT normalized to 1 and included 14–16 biological replicates per genotype. Normality of transcript and protein expression was assessed by D'Agostino & Pearson test and statistical comparison between groups was made using the nonparametric test Kruskal-Wallis with Dunn's post-hoc comparisons (GraphPad Prism v9.4.1, Graph Pad Software, San Diego, CA). Both assays lacked detectable signal in genomic, no-RT and no template controls.

### 2.4. Immunoblotting

Forebrain P3 membrane protein fractions were isolated from male and female WT, *Kcnb1*$^{C/+}$ and *Kcnb1*$^{C/C}$ mice at P58–83. Membrane fractions (50 μg) were separated on a 7.5% SDS-PAGE gel and transferred to nitrocellulose. Blots were probed with anti-$K_V$2.1 (K89/34) and anti-mortalin/GRP75 antibodies (Table 2). Alexa Fluor 790 goat anti-mouse antibodies (Table 2) were used to detect signal on an Odyssey imaging system (LI-COR). Relative protein levels were determined by densitometry using Image Studio (LI-COR) and expressed as a ratio of $K_V$2.1 to GRP75 with WT normalized to 1 and included 7–14 biological replicates per genotype. Normality of transcript and protein expression was assessed by D'Agostino & Pearson test and statistical comparison between groups was made using the nonparametric test Kruskal-Wallis with Dunn's post-hoc comparisons (GraphPad Prism).

### 2.5. Primary neuron cultures

P0–1 pups were rapidly genotyped using the RFLP genotyping assay as described above. Hippocampal neurons were harvested and plated on poly-D-lysine-coated coverslips (GG-12–1.5-PDL; Neuvitro, Vancouver WA) at a density of 0.25–0.30×10e$^6$ cells per well, maintained in Neurobasal medium (10888022; Gibco, Waltham, MA) supplemented with B-27 and Culture One (17504044 and A3320201; Gibco), with weekly half-volume media changes for 2–3 weeks. At least 2 independent cultures of 2 to 3 mice of each genotype were used for experiments.

### 2.6. Immunocytochemistry and image analyses

At DIV18–21, coverslips were fixed using Cytofix/Cytoperm (554,714; BD Biosciences, San Jose CA) containing 4% sucrose (*w*/*v*) followed by additional permeabilization with

0.25% Triton X100, when necessary. For Ankyrin G (AnkG) staining, two additional washes with 0.5% CHAPS (C3023; Sigma) in PermWash/PBS-T (PBS + Tween-20) for 5 min were conducted. Coverslips were blocked with 10% normal goat serum for 30 mins. Incubations with primary antibodies for $K_V2.1$ and Map2 or AnkG (Table 2) were performed in PermWash/PBS-T overnight at room temperature. Coverslips were then incubated with secondary antibodies (Table 2) diluted in PermWash/PBS-T + 10% NGS for 1–2 h, followed by DAPI staining for 10 min. Coverslips were then mounted on glass slides using prolong gold antifade reagent (P36934; Invitrogen).

Images were acquired using a Nikon W1 spinning disk confocal and Hamamatsu camera in the Center for Advanced Imaging at Northwestern University. ND2 files were processed and analyzed using NIS elements software (Nikon). Images were identically processed in Adobe Photoshop (v23.2.1) for figure production.

Approximately 15 to 23 axon initial segment (AIS) measurements, defined by Ankyrin G staining, were taken from 10 to 12 randomly selected images at 60× magnification. For each genotype, 3 to 4 coverslips were evaluated.

### 2.7. Electrophysiology

Whole-cell current clamp recordings were performed on DIV14–16 hippocampal pyramidal neurons. Pyramidal neurons were identified morphologically as cells with large pyramidal shaped cell bodies. All recordings were performed at room temperature using a Multiclamp 700B amplifier (Molecular Devices). External recording solution included (in mM): 155 NaCl, 3.5 KCl, 1.5 $CaCl_2$, 1 $MgCl_2$, 10 HEPES, 10 Glucose, with pH adjusted to 7.35 with NaOH. External recording solution also included 50 μM D-5AP (2-amino-5-phosphonopentanoic acid), 10 μM CNQX (6-cyano-7-nitroquinoxaline-2,3-dione) and 50 μM picrotoxin. Internal recording solution included (in mM): 120 $KMeSO_4$, 10 KCl, 5 MgATP, 0.4 Na-GTP, 5 $Na_2$-phosphocreatine with pH adjusted to 7.2 with KOH, and osmolarity adjusted to 280 mOsm/kg with sucrose. Current-clamp pulse generation and data collection were done with Clampex 10.4. For evoked action potential recordings, cells were held at −65 mV and action potentials were elicited by 2 s stimuli from −30–450 pA in 10 pA increments. Input resistance was calculated from a – 10 pA hyperpolarizing step. Input-output curves were compared by two-way ANOVA followed by Tukey's post-hoc comparisons. Resting membrane potential, action potential morphology, and input resistance were compared by one-way ANOVA followed by Tukey's post-hoc comparisons.

### 2.8. Open field assay

Baseline locomotor activity was measured in P70–91 male and female WT, *Kcnb1*$^{C/+}$ and *Kcnb1*$^{C/C}$ using an open field assay. Male and female mice were tested separately with at least a 1 h delay between sessions. Prior to behavioral testing, mice were acclimated in the behavior suite with white noise for 1 h. Each mouse was placed at the center of the open field arena (46 cm × 46 cm) and video monitored for 30 min. Video records were analyzed offline using Ethovision XT software (Noldus Information Technology, Leesburg, VA, USA) by a reviewer blinded to genotype. Distance traveled, number of zone transitions and % time spent in center of arena for each trial were compared with one or two-way ANOVA with

Tukey's post hoc comparisons. No difference in sex was detected, therefore groups were collapsed across sex ($n$ = 14–17 mice per genotype).

## 2.9. Seizure induction

Male and female mice were tested between 6 and 12 weeks of age by experimenters blinded to genotype. Separate cohorts of mice were used for each inducing agent.

**2.9.1. Flurothyl seizure induction—**Susceptibility to seizures induced by the chemoconvulsant flurothyl (Bis(2,2,2-trifluoroethyl) ether, Sigma-Aldrich, St. Louis, MO) was tested in male and female WT, *Kcnb1*$^{C/+}$ and *Kcnb1*$^{C/C}$ at P72–90 as previously described (Echevarria-Cooper et al., 2022; Hawkins et al., 2021). Briefly, mice were placed in a Plexiglas chamber (2.2 L) and flurothyl was introduced using a syringe pump (20 uL/min) and allowed to volatilize. Latencies to first myoclonic jerk, generalized tonic-clonic seizure (GTCS) with loss of posture, and time interval between these phases were compared using Kruskal-Wallis with Dunn's post-hoc comparisons. No difference in sex was detected, therefore groups were collapsed across sex ($n$ = 33–40 mice per genotype).

**2.9.2. Kainic acid seizure induction—**Susceptibility to seizures induced by the chemoconvulsant KA (kainic acid, Cat #0222, Tocris Bioscience, Minneapolis, MN) was tested in WT, *Kcnb1*$^{C/+}$ and *Kcnb1*$^{C/C}$ mice at P41–50. KA dissolved in saline was administered by intraperitoneal injection (25 mg/kg) and mice were video recorded for 2 h. Videos were scored offline by reviewers blinded to genotype using a modified Racine scale (Racine, 1972) (1-behavioral arrest; 2- forelimb and/or Straub tail, facial automatisms; 3-automatisms, including repetitive scratching, circling, forelimb clonus without falling; 4- forelimb clonus with rearing and/or falling, barrel roll; 5- repetition of stage 4; 6-generalized tonic-clonic seizure, wild running and/or jumping; 7- death). Latencies to the first occurrence of each stage and the highest seizure stage reached within 5 min bins were determined from video records by reviewers blinded to genotype. Latency to death following KA injection was compared by log-rank Mantel-Cox time to event analysis. Severity within time bins was compared between mutant alleles and WT by two-way ANOVA with Tukey's post hoc comparisons. No difference in sex was identified, therefore groups were collapsed across sex ($n$ = 12–19 mice per genotype).

## 2.10. Video-EEG monitoring

At 19–21 weeks of age, male and female WT, *Kcnb1*$^{C/+}$ and *Kcnb1*$^{C/C}$ mice were implanted with EEG headmounts (8201, Pinnacle Technology, Lawrence, KS) under ketamine/xylazine anesthesia. Headmounts with four stainless steel screws that served as cortical surface electrodes were affixed to the skull with glass ionomer cement. Anterior screw electrodes were 0.5–1 mm anterior to bregma and 1 mm lateral from the midline. Posterior screws were 4.5–5 mm posterior to bregma and 1 mm lateral from the midline. EEG1 represents recordings from right posterior to left posterior (interelectrode distance ≈2 mm) and EEG2 represents recordings from right anterior to left posterior (interelectrode distance ≈5 mm). The left anterior screw served as the ground connection. Following at least 48 h of recovery, tethered EEG and video data were continuously collected for 7 to 14 days from freely moving mice with Sirenia acquisition software (Pinnacle Technology). EEG data between

0.5 and 200 Hz were acquired at a sampling rate of 400 Hz. Raw data was notch filtered around 60 and 120 Hz prior to analysis. EEG records were assigned a randomly generated code to blind reviewers to genotype during analysis. On average, 78 h of EEG data were analyzed from each subject (WT: 70–120 h/mouse, $n = 4$ mice; *Kcnb1*$^{C/+}$: 70–73 h/mouse, $n = 6$ mice; *Kcnb1*$^{C/C}$: 70–76 h/mouse, $n = 5$ mice). Video-EEG records were manually reviewed for electrographic seizures (≥2× baseline; ≥10 s; evolution in frequency and amplitude) and epileptiform discharges, including SWD trains. SWD trains were defined as having regular, rhythmic sharp spike and slow wave components with ≥1 SWD per second continuing for ≥5 s, between 1 and 2.5 Hz frequencies.

RMS, cyclic frequency, and semi-automated spike-wave detection were performed using LabChart v8.1.19 (ADinstruments). After each file was manually reviewed, more focused, 6-h epochs (3–9 pm) from three days ($n = 18$ h/mouse) were extracted and analyzed. RMS and cyclic frequencies were calculated in LabChart data pad for each epoch. RMS value was considered average baseline for each file. SWDs were classified by the following: Spike with slow wave morphology (1–2.5 Hz), spike amplitude ≥x4 RMS and average duration of 200–500 msec. Table 4 summarizes EEG characteristics for each mouse.

### 2.11. Statistical analysis

Table 3 summarizes statistical tests used for all comparisons along with computed values. Values for post-hoc tests are reported in the results and figure legends. No significant differences were detected between sexes on reported measures; thus, groups were collapsed across sex.

## 3. Results

Previous functional studies showed altered voltage-dependence of $K_V2.1$ channels incorporating the R306C variant (Kang et al., 2019; Fernández-Mariño, 2023; Saitsu, 2015). In transfected CHO-K1 cells, despite normal cell surface expression of $K_V2.1$, R306C effects ranged from loss of delayed rectifier potassium currents when singly expressed to partial loss of function and altered voltage-dependence when co-expressed with WT to approximate the heterozygous condition (Kang et al., 2019; Fernández-Mariño, 2023; Saitsu, 2015). Transfection into cultured cortical pyramidal neurons resulted in lower sensitivity and cooperativity of the voltage sensor and severely impaired repetitive firing (Saitsu et al., 2015). These effects on channel function are unique compared to other variants modeled in mouse to date, including the dominant-negative pore variant *Kcnb1*$^{G379R}$, the trafficking defective variant *Kcnb1*$^{R312H}$, *Kcnb1* knockout mice (*Kcnb1*$^{-/-}$), or premature termination codon *Kcnb1*$^{fs}$ mice (Bortolami et al., 2022; Hawkins et al., 2021; Speca et al., 2014). Furthermore, the R306C variant has a high rate of recurrence in patient cohorts. Taken together, these observations made R306C a high priority variant for in vivo modeling.

### 3.1. Generation and initial characterization of Kcnb1$^{R306C}$ mice

*Kcnb1*$^{R306C}$ mice on the C57BL/6J inbred strain were generated using CRISPR/Cas9 to introduce the modification of arginine 306 (same codon number in human and mouse) by HDR. Sequencing chromatograms of *Kcnb1* genomic PCR products showing the WT and

R306C variant alleles are shown in Fig. 1A. *Kcnb1*$^{R306C}$ mice were born at the expected Mendelian ratios and there was no difference in survival compared to WT littermates (Supplementary Fig. S1). Additionally, we did not observe excess/unexpected deaths in our colony maintenance of this line over 4 years. Expression analyses of bulk forebrain tissue revealed no significant differences in the *Kcnb1* transcript or $K_V2.1$ protein expression across the three genotypes: WT, heterozygous *Kcnb1*$^{R306C/+}$ (*Kcnb1*$^{C/+}$ or C/+) and homozygous *Kcnb1*$^{R306C/R306C}$ (*Kcnb1*$^{C/C}$ or C/C) (Fig. 1B–D; $p > 0.2$, Kruskal-Wallis). Thus, the R306C variant does not affect $K_V2.1$ expression levels, consistent with prior studies in CHO-K1 cells (Kang et al., 2019).

### 3.2. Normal expression and localization of $K_V2.1$ in R306C cultured hippocampal neurons

To assess the impact of the *Kcnb1*$^{R306C}$ variant on $K_V2.1$ expression in neurons, we performed immunolabeling of cultured hippocampal neurons (DIV16–18) isolated from WT, *Kcnb1*$^{C/+}$ and *Kcnb1*$^{C/C}$ mice. The *Kcnb1*$^{R306C}$ variant had no overt effect on expression or subcellular localization of $K_V2.1$. Robust clustering in the soma and proximal processes was present across all genotypes, indicating that the R306C variant does not impair localization or cluster formation (Fig. 2A). Co-immunolabeling with MAP2 or Ankyrin-G was consistent with $K_V2.1$ localization in proximal dendrites and AIS, respectively, across all genotypes (Fig. 2A). One hallmark of $K_V2.1$ expression in neurons is its early and robust expression in the proximal AIS, a critical site for regulation of neuronal polarity. Therefore, we measured AIS length to determine if *Kcnb1*-p.R306C affected AIS maturation. AIS length measurements were not different across genotypes (Fig. 2B) ($F(2,177) = 1.807$, $p = 0.1671$, one-way ANOVA).

### 3.3. Altered neuronal excitability in R306C cultured hippocampal neurons

We compared neuronal excitability of cultured hippocampal neurons (DIV 14–16) from WT, *Kcnb1*$^{C/+}$ and *Kcnb1*$^{C/C}$ mice. We observed that neurons from *Kcnb1*$^{C/+}$ were hypoexcitable compared to WT neurons, consistent with previously reported results (Fig. 3A,B) (Saitsu et al., 2015). Interestingly, neurons from *Kcnb1*$^{C/C}$ animals were hyperexcitable at strong stimuli compared to both WT and *Kcnb1*$^{C/+}$ neurons (Fig. 3 A,B). Comparison of resting membrane potential showed that neurons from *Kcnb1*$^{C/+}$ animals were significantly depolarized compared to WT, as was action potential threshold (Fig. 3C, D). Additionally, action potentials were wider, with slower upstroke and downstroke velocity for both *Kcnb1*$^{C/+}$ and *Kcnb1*$^{C/C}$ neurons compared to WT, although amplitudes were similar (Fig. 3E–H). Neurons from these animals also showed a significantly smaller fast-afterhyperpolarization compared to WT neurons (Fig. 3I). Lastly neurons from *Kcnb1*$^{C/+}$ and *Kcnb1*$^{C/C}$ animals showed lower input resistance compared to WT neurons (Fig. 3J).

### 3.4. Locomotor hyperactivity in Kcnb1$^{R306C}$ mice

Differences in locomotor activity levels between *Kcnb1*$^{R306C}$ and WT mice was evident in their home cages during routine husbandry and was reminiscent of the profound hyperactivity observed in *Kcnb1*$^{G379R}$ and *Kcnb1*$^{-/-}$ mice (Hawkins et al., 2021; Speca et al., 2014). To quantify this effect, we measured baseline locomotor activity in a 30-min open field assay. Both *Kcnb1*$^{C/+}$ and *Kcnb1*$^{C/C}$ mice traveled farther in the open field than WT littermate controls ($F(2,44) = 20.6$, $p < 0.0001$, one-way ANOVA). WT mice traveled

an average distance of 121.4 ± 4.1 m, while *Kcnb1*$^{C/+}$ and *Kcnb1*$^{C/C}$ traveled 155.1 ± 5.4 and 164.7 ± 5.4 m, respectively (Fig. 4A,E). Distance traveled was consistently elevated over the course of the 30-min period in *Kcnb1*$^{C/+}$ and *Kcnb1*$^{C/C}$ mice compared to WT, while all genotypes showed similar short-term habituation (Fig. 4B). The number of zone transitions and time spent in the arena center were assessed as a rudimentary evaluation for anxiety within the open field setting. The total number of zone transitions was affected by *Kcnb1* genotype ($F(2,44) = 4.86$ $p < 0.02$; one-way ANOVA). *Kcnb1*$^{C/+}$ mice crossed the testing arena an average of 207.4 ± 13.5 times in 30 min ($p < 0.02$), while WT and *Kcnb1*$^{C/C}$ mice crossed an average of 150.6 ± 10.8 times and 192.5 ± 16.6, respectively (Fig. 4C, E). However, there was no difference between genotypes for the percentage of time spent in the center of the arena (Fig. 4D).

### 3.5. Altered seizure susceptibility in Kcnb1$^{R306C}$ mice

Previous studies showed enhanced seizure susceptibility in *Kcnb1*$^{G379R}$ and *Kcnb1*$^{-/-}$ knockout mice (Hawkins et al., 2021; Speca et al., 2014). In order to compare with other *Kcnb1* mouse models, we asked how the R306C variant affects seizure susceptibility using two chemoconvulsants, flurothyl and KA. First, we used the $GABA_A$ antagonist flurothyl to induce a stereotyped progression that begins with a myoclonic jerk (MJ) as the first seizure sign and progresses to a GTCS. Latency for flurothyl-induced seizures was affected differently by mutant allele dosage. *Kcnb1*$^{C/+}$ mice exhibited longer latencies to both the MJ (127 s 95% CI [115, 141]) and GTCS, (188 s 95% CI [170, 205]), compared to WT mice (MJ: 113 s 95% CI [101,121]; GTCS: 173 s 95% CI [158, 179]) (Fig. 5A–B). In contrast, *Kcnb1*$^{C/C}$ mice showed no difference in MJ latency relative to WT, but had a ≈ 15% shorter latency to the GTCS (132 s 95% CI [128, 146]), (Fig. 5A–B). Comparison of the time interval between MJ and GTCS showed that *Kcnb1*$^{C/C}$ mice progressed quickly between the stages, with a median time of 27 s 95% CI [17, −50], while WT and *Kcnb1*$^{C/+}$ exhibited similar median times of 58 s 95% CI [45, 68] and 53 s 95% CI [40, 64], respectively (Fig. 5C).

Next, we evaluated susceptibility to seizures induced by the glutamatergic agonist KA in a separate cohort of mice. Seizure intensity following KA administration was assessed over a 2-h period using a modified Racine scale, scoring for latency to first occurrence of each stage and for the highest stage reached within 5-min bins (Fig. 5D–F). There were no differences in latency to stages 1 or 2 between any genotype. However, for stages 3–7, *Kcnb1*$^{C/C}$ mice had a shorter average latency compared to WT and were quicker to reach stage 6 compared to *Kcnb1*$^{C/+}$. (Fig. 5D). *Kcnb1*$^{C/+}$ mice had shorter latencies to stages 5 and 6 compared to WT mice (Fig. 5D). Comparison of the survival rates of WT, *Kcnb1*$^{C/+}$ and *Kcnb1*$^{C/C}$ after KA administration revealed that all *Kcnb1*$^{C/C}$ and ≈75% of *Kcnb1*$^{C/+}$ died within 2 h following KA administration, while only ≈25% of WT mice died (Fig. 5E–F). The median latency to death was 31.6 min in *Kcnb1*$^{C/C}$ and 42.5 min for *Kcnb1*$^{C/+}$ mice, while ≈75% of WT mice survived for at least 2-h post-KA (Fig. 5E–F).

### 3.6. EEG abnormalities in Kcnb1$^{R306C}$ mice

Adult *Kcnb1*$^{C/C}$ mice were sporadically observed exhibiting spontaneous GTCS in their home cages (Supplementary Video S4). To systematically evaluate electrographic events and

quantify EEG properties, we collected synchronized video-EEG data from WT, *Kcnb1*$^{C/+}$ and *Kcnb1*$^{C/C}$ mice at ≈20 weeks of age. Video-EEG was continually recorded for 7–14 days. Manual review of approximately 78 h of EEG per mouse revealed a single spontaneous generalized seizure in a *Kcnb1*$^{C/+}$ mouse (1 in 427 total hours; $n = 6$ mice) (Fig. 6A; Supplementary Video S5, Table 4), as well as a single generalized seizure in a *Kcnb1*$^{C/C}$ mouse (1 in 363 total hours; $n = 5$ mice). Low GTCS incidence was not unexpected, as previous work from our lab showed that other *Kcnb1* mutant lines had relatively low GTCS frequency (Hawkins et al., 2021; Speca et al., 2014). Furthermore, GTCS witnessed during routine handling or husbandry were very rare.

Beyond the rare spontaneous GTCS events, EEGs were markedly abnormal in *Kcnb1*$^{R306C}$ mice. Both *Kcnb1*$^{C/+}$ and *Kcnb1*$^{C/C}$ mice exhibited abundant epileptiform activity consisting of recurrent trains of slow spike-wave complexes of varying durations and overall slowed interictal activity on EEG (Figs. 6B–G, 7, Table 4). To quantify these observations, we performed focused analysis from 3 to 9 PM on 3 separate days totaling 18 h of EEG traces per mouse (Table 4, Fig. 7A–C). Root mean square (RMS) was calculated for each 6-h epoch to determine average amplitude baseline (Fig. 7A, E). WT mice had an average RMS value of 11.5 ± 0.64 μV, while both *Kcnb1*$^{C/+}$ (25.1 ± 2.9 μV) and *Kcnb1*$^{C/C}$ (23.9 ± 3.5 μV) mice had comparatively elevated average RMS values ($F(2,37) = 5.322$ $p = 0.0093$; Two-way ANOVA), likely due to the frequently observed high amplitude spiking. Cyclic frequency was calculated to assess the overall rate of wave patterns in each 6-h epoch (Fig. 7B,E). *Kcnb1*$^{C/C}$ mice exhibited the lowest average cyclic frequency of 4.5 ± 0.3 Hz. *Kcnb1*$^{C/+}$ mice exhibited a slightly faster rate of 4.9 ± 0.7 Hz, while WT averaged 5.3 ± 0.1 Hz (($F(2,37) = 3.548$ $p = 0.0389$; Two-way ANOVA).

Due to the abundant observations of extended spike trains identified in the ~78 h manually reviewed files, we calculated spike frequency from the more focused, 6-h EEG epochs and spike train durations from the full traces. SWD trains were more often identified during periods of rest, but many did occur during wakefulness and coincided with circling or behavioral arrest with head bobbing (Fig. 6B–G). SWDs were counted and classified using Spike Detector (Lab Chart), by the following characteristics: spike with slow wave morphology (1–2.5 Hz); spike amplitude ≥4× RMS; and duration of 200–500 msec. Both *Kcnb1*$^{C/+}$ and *Kcnb1*$^{C/C}$ SWD rates were elevated compared to WT (Fig. 7C, D) ($p < 0.0001$, Kruskal-Wallis One-Way ANOVA). WT mice had low occur-rences of SWDs, averaging 3.3 ± 0.6 per hr, and no SWD trains were identified in ~377 h of manually reviewed EEG (Fig. 7C, D). In *Kcnb1*$^{C/+}$ recordings, 4 of 6 mice collectively experienced 69 instances of SWD trains ranging from 6 s to 140 min (Figs. 6B–D, 7D). For focused spike counting, *Kcnb1*$^{C/+}$ exhibited an average rate of 55.6 ± 30.5 SWD per hr (Fig. 7C). In *Kcnb1*$^{C/C}$ recordings, 3 of 5 mice collectively experienced 45 instances of SWD trains, ranging from 19 s to 108 min, (Figs. 6E–G, 7D). For focused spike counting, *Kcnb1*$^{C/C}$ exhibited an average SWD rate of 71.2 ± 26.1 SWD per hr (Fig. 7C).

Furthermore, we used spectral analysis to examine interictal EEG during 1-min epochs free of SWDs and artifacts, which revealed alterations in background EEG between WT and *Kcnb1*$^{R306C}$ mice. Relative to WT, *Kcnb1*$^{C/+}$ mice had elevated power in the beta frequency band during both active periods and at rest (Supplementary Fig. S2). Compared to WT,

*Kcnb1*$^{C/C}$ mice had elevated power in the delta and theta frequency bands during active periods, and in the delta and beta frequency bands at rest (Supplementary Fig. S2).

## 4. Discussion

*KCNB1*-p.R306C is the one of the most recurrent variants identified to date in individuals with *KCNB1* encephalopathy, and is associated with mild to severe global developmental delays, behavioral disorders, and a diverse spectrum of epilepsy that includes infantile spasms, GTC, myoclonic, tonic, focal, and absence seizures (Bar et al., 2020a; de Kovel et al., 2017; Kang et al., 2019; Marini et al., 2017; Saitsu et al., 2015). Previous in vitro characterization of R306C showed altered sensitivity and cooperativity of the channel voltage-sensor and impaired capacity for repetitive firing, which can disrupt neuronal circuitry and result in clinical manifestations of developmental encephalopathy (Fernández-Mariño et al., 2023; Kang et al., 2019; Saitsu et al., 2015). We and others have previously generated and characterized mouse models of *Kcnb1* encephalopathy, including the missense variants *KCNB1*-p.G379R, *KCNB1*-p.R312H, as well as a *Kcnb1*$^{-/-}$ knock-out and frameshift alleles (Bortolami et al., 2022; Hawkins et al., 2021; Speca et al., 2014). The existing *Kcnb1* mouse models recapitulated *KCNB1* encephalopathy phenotypes, including spontaneous seizures, EEG abnormalities, learning deficits and hyperactivity (Bortolami et al., 2022; Hawkins et al., 2021; Speca et al., 2014). While *Kcnb1*$^{G379R}$, *Kcnb1*$^{R312H}$, and *Kcnb1* null and frameshift models are informative LoF alleles, the *Kcnb1*$^{R306C}$ mutation represents a recurrent variant with different underlying mechanisms and biological impacts. Thus, this new model expands the allelic series of *Kcnb1* mouse models, which may help establish nuanced genotype-phenotype correlations.

Previous results from our laboratory demonstrated that the R306C variant exhibited normal protein expression level and cell-surface trafficking in CHO cells (Kang et al., 2019). Consistent with this, *Kcnb1*$^{C/+}$ and *Kcnb1*$^{C/C}$ mice did not have significant changes in transcript, or protein expression relative to WT (Fig. 1). Moreover, there was no difference in subcellular localization or clustering in *Kcnb1*$^{C/+}$ and *Kcnb1*$^{C/C}$ mice compared to WT (Fig. 2). In contrast, the *Kcnb1*$^{G379R}$ and *Kcnb1*$^{R312H}$ mouse models had substantial, genotype-dosage dependent reduction in $K_V2.1$ expression, as well as dominant-negative effects on $K_V2.1$ macromolecular complexes (Bortolami et al., 2022; Hawkins et al., 2021). Thus, the *Kcnb1*$^{R306C}$ phenotype is likely a direct result of altered voltage sensing rather than diminished protein expression and/or localization. This is an important distinction as voltage-sensing dysfunction may be amenable to different therapeutic approaches than diminished protein expression (Haq et al., 2022; Tian et al., 2022). Consistent with this, hippocampal pyramidal neurons isolated from *Kcnb1*$^{C/+}$ and *Kcnb1*$^{C/C}$ mice displayed alterations in passive membrane properties and intrinsic excitability.

Both *Kcnb1*$^{C/+}$ and *Kcnb1*$^{C/C}$ mice exhibited open field hyperactivity. This is consistent with previous reports of hyperactivity in *Kcnb1*$^{G379R}$ and *Kcnb1*$^{-/-}$ mice (Hawkins et al., 2021; Speca et al., 2014), as well as clinical reports of attention-deficit/hyperactivity disorder or hyperactivity with inattention in numerous cases of *KCNB1* encephalopathy (Bar et al., 2020a; de Kovel et al., 2017; Kang et al., 2019; Marini et al., 2017; Torkamani et al., 2014). There was no significant effect of R306C allele dosage on hyperactivity, in contrast

to G379R that consistently had more severe neurobehavioral phenotypes in homozygotes compared to heterozygous littermates (Hawkins et al., 2021). This again supports the notion of differential effects of altered voltage sensing versus dominant negative in *Kcnb1* disease.

Seizure susceptibility was altered in $Kcnb1^{R306C}$ mice relative to WT, although there were differential effects depending on genotype and chemoconvulsant. In response to KA, we observed an allele dosage effect, with $Kcnb1^{C/C}$ mice being more severe than both $Kcnb1^{C/+}$ and WT, and $Kcnb1^{C/+}$ having intermediate sensitivity to KA. In contrast, latency to flurothyl-induced seizures was differentially modulated in $Kcnb1^{C/+}$ versus $Kcnb1^{C/C}$ mice. Latencies relative to WT were longer in $Kcnb1^{C/+}$ heterozygotes, while they were shorter in $Kcnb1^{C/C}$ homozygotes. The paradoxical relationship was mirrored in the intrinsic excitability of hippocampal pyramidal neurons, with hypoexcitability of neurons from $Kcnb1^{C/+}$ and hyperexcitability of neurons $Kcnb1^{C/C}$ mice at high stimulation frequencies. The genotype-dependence of flurothyl response and neuronal excitability alterations suggests a fundamental difference between having mutant-only homotetramers in $Kcnb1^{C/C}$ mice versus $Kcnb1^{C/+}$ mice having a mixture of possible $K_V2.1$ tetramer populations that may include WT-only and mutant-only homotetramers, as well as heterotetramers of WT and R306C with various stoichiometric ratios (Kang et al., 2019). When expressed as a homotetramer, R306C channels had complete loss-of-function when examined with a physiologically relevant holding potential of −80 mV (Kang et al., 2019). Consistent with this, the observed seizure susceptibility in $Kcnb1^{C/C}$ homozygous mice was similar to $Kcnb1^{-/-}$ mice, which also had a ≈ 15% reduction in flurothyl threshold relative to WT (Hawkins et al., 2021; Speca et al., 2014). In contrast, $Kcnb1^{G379R}$ mice with a dominant-negative variant had a more pronounced response to flurothyl compared to $Kcnb1^{C/C}$ mice. Compared to WT, $Kcnb1^{G379R/G379R}$ homozygotes had a 37% reduction in flurothyl threshold, while $Kcnb1^{G379R/+}$ heterozygotes had a ≈ 15% reduction (Hawkins et al., 2021). The magnitude of threshold reduction compared to these other *Kcnb1* lines suggests that $Kcnb1^{C/C}$ results in loss-of-function rather than a dominant-negative effect. Previous work showed that repetitive action potential firing was completely suppressed in cortical pyramidal neurons co-expressing WT and R306C channels (Saitsu et al., 2015). This, coupled with differences in mechanisms of seizure induction by KA versus flurothyl, may underlie the observed differential response in $Kcnb1^{C/+}$ heterozygotes. Flurothyl acts as a GABA antagonist, suppressing presynaptic GABA release, while KA acts on both pre- and post-synaptic receptors to suppress presynaptic GABA release *and* enhance postsynaptic activation of glutamatergic neurons (Falcón-Moya et al., 2018). Thus, despite the failure of action potential firing in heterozygous pyramidal neurons, the KA condition provides an excitatory drive that is absent in the flurothyl condition.

Although seizure susceptibility can give us a measure of altered excitatory/inhibitory balance, the role of $K_V2.1$ as a dynamically regulated homeostatic modulator of neuronal excitability makes it challenging to directly translate these acute effects to epilepsy propensity. Thus, we performed EEG analysis to study epileptiform activity and background EEG properties. Among individuals with the *KCNB1*-p. R306C variant, common EEG findings are diffuse polyspike waves, high amplitude spike wave complexes and continuous spike and wave during sleep (CSWS) (de Kovel et al., 2017; Marini et al., 2017). $Kcnb1^{C/+}$ and $Kcnb1^{C/C}$ mice were found to have markedly abnormal EEG patterns, including many

of the above listed characteristics. Most evident in the EEG traces were lengthy, rhythmic, high-amplitude, low frequency spike wave trains, reminiscent of the 1 to 2.5 Hz slow spike and wave activity characteristic of Lennox Gastaut syndrome (Gastaut et al., 1966; Markand, 1977; Niedermeyer, 1969). Interestingly, patients with slow spike-wave activity show high convulsive thresholds to intravenous pentylenetetrazol (Gastaut et al., 1966), similar to our observations of high thresholds in *Kcnb1*$^{C/+}$ mice. The slow spike and wave events sometimes lasted for hours, while the mouse was inactive. Although we cannot definitively conclude that these events recapitulate CSWS, the similarity is striking. Previous work identified spike and wave complexes lasting up to 15 min in *Kcnb1*$^{G379R}$ mice, while spontaneous seizure activity was absent from recordings in *Kcnb1*$^{-/-}$ mice (Hawkins et al., 2021; Speca et al., 2014); thus, the frequency and duration of these complexes in *Kcnb1*$^{R306C}$ mice was unprecedented. The recently reported *KCNB1*-p. R312H mouse model also showed convulsive and non-convulsive seizures, including long duration seizure activity (4–5 min) defined by sustained rhythmic synchronous discharges, providing further support that the persistent spiking identified in *Kcnb1*$^{R306C}$ is pathogenic (Bortolami et al., 2022). Future studies using high-dose benzodiazepines, valproate, or corticosteroids would be useful to determine if the rhythmic high-amplitude spike wave trains in the *Kcnb1*$^{R306C}$ mouse model can be attenuated with drugs commonly used for CSWS (Sánchez Fernández et al., 2014).

Limitations of this study that were not in the scope of this manuscript and will be addressed in the future include the following. Our analysis of subcellular localization and AIS maturation was a snapshot at DIV16–18, and therefore does not preclude the possibility of impaired maturation occurring at a later time point. We documented behavioral hyperactivity in the open field assay, consistent with the profound hyperactivity reported for other *Kcnb1* alleles; however, future studies will be needed to more thoroughly examine neurobehavior. In addition, our EEG recordings did not include EMG or accelerometer data necessary for systematically staging sleep, an essential feature for CSWS diagnosis; thus, we could not definitively classify the long bouts of rhythmic high-amplitude spike wave trains accompanied by behavioral immobility as CSWS. Finally, effects at the level of circuit, network, and non-conducting roles of $K_V2.1$ were not probed in this study and future studies will be necessary to determine their contributions to clinical phenotypes.

## 5. Conclusions

In summary, we generated and characterized a novel knock-in mouse model of *KCNB1* encephalopathy due to voltage-sensor dysfunction of $K_V2.1$ channels. This represents a major category of dysfunction observed for channelopathies and the model will be a valuable resource for understanding disease pathophysiology and evaluating potential therapies.

## Supplementary Material

Refer to Web version on PubMed Central for supplementary material.

## Acknowledgements

We thank *KCNB1* families for their support, and Colette Brill-Forman for technical assistance. The genetically engineered mice were generated with the assistance of Lynn Doglio and Eugene Wyatt in Northwestern University Transgenic and Targeted Mutagenesis Laboratory. Imaging work was performed at the Northwestern University Center for Advanced Microscopy generously supported by NCI CCSG P30 CA060553 awarded to the Robert H Lurie Comprehensive Cancer Center. This work was supported by generous philanthropic donations and the National Institutes of Health grant U54 NS108874 (ALG, JAK).

## Data availability

Data will be made available on request.

## Abbreviations:

| | |
|---|---|
| **AnkG** | Ankyrin G |
| **AIS** | axon initial segment |
| **flurothyl** | Bis(2,2,2-trifluoroethyl) ether |
| **CI** | confidence interval |
| **DIV** | days in vitro |
| **EEG** | electroencephalogram |
| **FFT** | fast fourier transform |
| **GTCS** | generalized tonic-clonic seizure |
| **gRNA** | guide RNA |
| **HDR** | Homology directed repair |
| **ICC** | immunocytochemistry |
| **IDT** | Integrated DNA Technologies, Inc. |
| **KA** | kainic acid |
| **LoF** | loss-of-function |
| **MJ** | myoclonic jerk |
| **PBS-T** | PBS + tween-20 |
| **PAM** | protospacer adjacent motif |
| **PSD** | Power spectral density |
| **RFLP** | restriction fragment length polymorphism |
| **RMS** | Root mean square |
| **RNP** | ribonucleotide protein complex |

| | |
|---|---|
| **ssODN** | single-stranded donor oligonucleotide |
| **SPF** | specific pathogen free |
| **SWD** | spike-wave discharge |
| **WB** | western blot |
| **WT** | wildtype |

## References


Aida T, et al. , 2014. Translating human genetics into mouse: the impact of ultra-rapid in vivo genome editing. Dev. Growth Differ 56, 34–45. [PubMed: 24444057]

Bar C, et al. , 2020a. Expanding the genetic and phenotypic relevance of KCNB1 variants in developmental and epileptic encephalopathies: 27 new patients and overview of the literature. Hum. Mutat 41, 69–80. [PubMed: 31513310]

Bar C, et al. , 2020b. Developmental and epilepsy spectrum of KCNB1 encephalopathy with long-term outcome. Epilepsia. 61, 2461–2473. [PubMed: 32954514]

Bortolami A, et al. , 2022. Integrin-KCNB1 potassium channel complexes regulate neocortical neuronal development and are implicated in epilepsy. Cell Death Differ 30, 687–701. [PubMed: 36207442]

Catacuzzeno L, Franciolini F, 2022. The 70-year search for the voltage-sensing mechanism of ion channels. J. Physiol 600, 3227–3247. [PubMed: 35665931]

Chesselet MF, Carmichael ST, 2012. Animal models of neurological disorders. Neurotherapeutics. 9, 241–244. [PubMed: 22460561]

de Kovel CGF, et al. , 2017. Neurodevelopmental disorders caused by de novo variants in KCNB1 genotypes and phenotypes. JAMA Neurol. 74, 1228–1236. [PubMed: 28806457]

Echevarria-Cooper DM, et al. , 2022. Cellular and behavioral effects of altered NaV1.2 sodium channel ion permeability in Scn2aK1422E mice. Hum. Mol. Genet 31, 2964–2988. [PubMed: 35417922]

Falcón-Moya R, et al. , 2018. Kainate receptors: role in epilepsy. Front. Mol. Neurosci 11, 217. [PubMed: 29988380]

Fernández-Mariño AI, et al. , 2023. Inactivation of the Kv2.1 channel through electromechanical coupling. Nature. 622, 410–417. [PubMed: 37758949]

Gastaut H, et al. , 1966. Childhood epileptic encephalopathy with diffuse slow spike-waves (otherwise known as “petit mal variant”) or Lennox syndrome. Epilepsia. 7, 139–179. [PubMed: 4959714]

Haq I, et al. , 2022. Precision medicine based on CFTR genotype for people with cystic fibrosis. Pharmgenomics Pers Med. 15, 91–104. [PubMed: 35153502]

Hawkins NA, et al. , 2021. Epilepsy and neurobehavioral abnormalities in mice with a dominant-negative KCNB1 pathogenic variant. Neurobiol. Dis 147, 105141. [PubMed: 33132203]

Kang SK, et al. , 2019. Spectrum of KV 2.1 dysfunction in KCNB1-associated neurodevelopmental disorders. Ann. Neurol 86, 899–912. [PubMed: 31600826]

Marini C, et al. , 2017. Clinical features and outcome of 6 new patients carrying de novo KCNB1 gene mutations. Neurol. Genet 3, e206. [PubMed: 29264397]

Markand ON, 1977. Slow spike-wave activity in EEG and associated clinical features: often called ‘Lennox’ or ‘Lennox-Gastaut’ syndrome. Neurology. 27, 746–757. [PubMed: 407485]

Murakoshi H, Trimmer JS, 1999. Identification of the Kv2.1 K+ channel as a major component of the delayed rectifier K+ current in rat hippocampal neurons. J. Neurosci 19, 1728–1735. [PubMed: 10024359]

Niedermeyer E, 1969. The Lennox-Gastaut syndrome: a severe type of childhood epilepsy. Dtsch. Z. Nervenheilkd 195, 263–282. [PubMed: 4979309]

Percie du Sert N, et al. , 2020. The ARRIVE guidelines 2.0: updated guidelines for reporting animal research. Br. J. Pharmacol 177, 3617–3624. [PubMed: 32662519]

Platt RJ, et al. , 2014. CRISPR-Cas9 knockin mice for genome editing and cancer modeling. Cell. 159, 440–455. [PubMed: 25263330]

Racine RJ, 1972. Modification of seizure activity by electrical stimulation. II. Motor seizure. Electroencephalogr. Clin. Neurophysiol 32, 281–294. [PubMed: 4110397]

Saitsu H, et al. , 2015. De novo KCNB1 mutations in infantile epilepsy inhibit repetitive neuronal firing. Sci. Rep 5, 15199. [PubMed: 26477325]

Sánchez Fernández I, et al. , 2014. Treatment for continuous spikes and waves during sleep (CSWS): survey on treatment choices in North America. Epilepsia. 55, 1099–1108. [PubMed: 24917485]

Scheffer IE, Liao J, 2020. Deciphering the concepts behind “epileptic encephalopathy” and “developmental and epileptic encephalopathy”. Eur. J. Paediatr. Neurol 24, 11–14. [PubMed: 31926847]

Speca DJ, et al. , 2014. Deletion of the Kv2.1 delayed rectifier potassium channel leads to neuronal and behavioral hyperexcitability. Genes Brain Behav. 13, 394–408. [PubMed: 24494598]

Thiffault I, et al. , 2015. A novel epileptic encephalopathy mutation in KCNB1 disrupts Kv2.1 ion selectivity, expression, and localization. J. Gen. Physiol 146, 399–410. [PubMed: 26503721]

Tian F, et al. , 2022. Epilepsy phenotype and response to KCNQ openers in mice harboring the Kcnq2 R207W voltage-sensor mutation. Neurobiol. Dis 174, 105860. [PubMed: 36113748]

Torkamani A, et al. , 2014. De novo KCNB1 mutations in epileptic encephalopathy. Ann. Neurol 76, 529–540. [PubMed: 25164438]

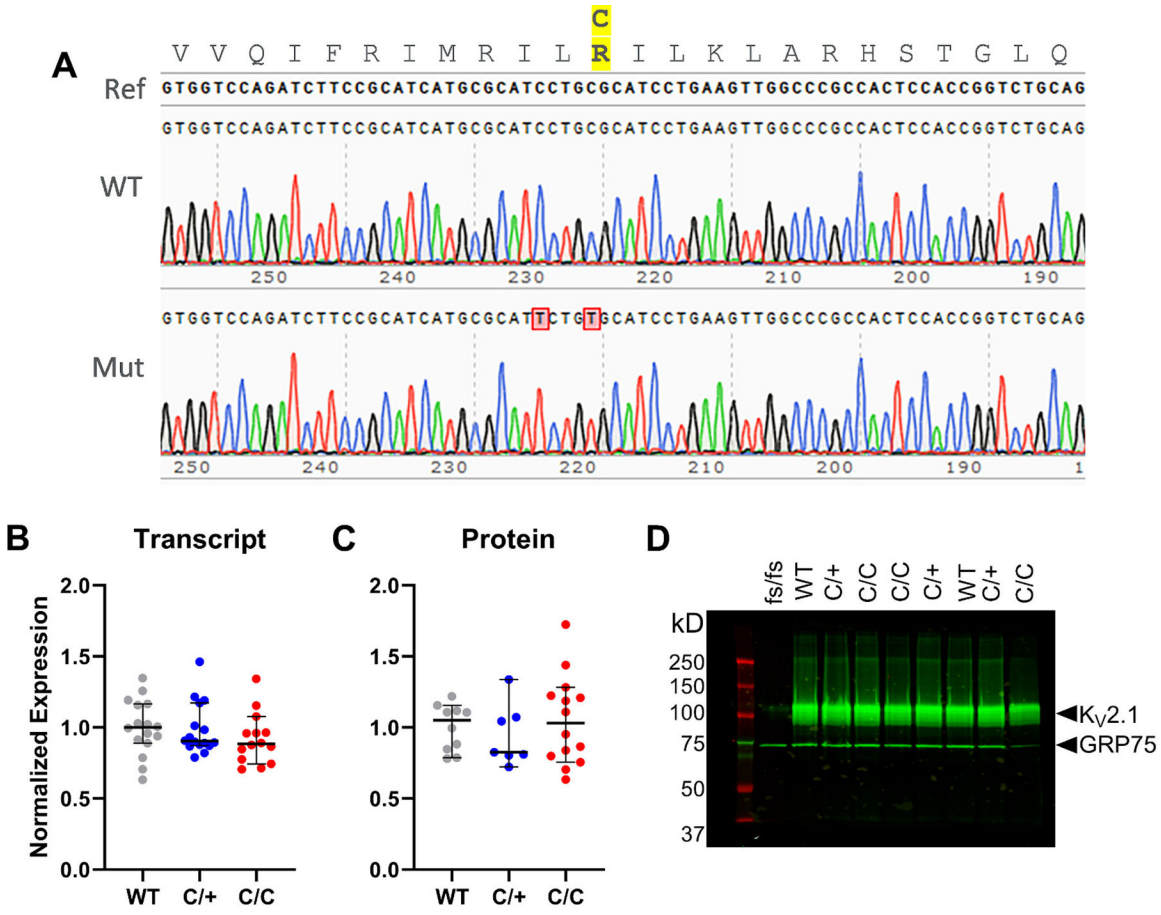


**Fig. 1.**

Characterization of *Kcnb1*-p.R306C variant allele. (A) Chromatogram confirmation of *Kcnb1* R306C genomic PCR product. Genomic PCR products were TOPO cloned and Sanger sequenced. The top trace represents a WT allele with 100% identity to the mouse C57BL/6J reference genome (GRCm39). The bottom trace shows a mutated allele (Mut) that encodes p.R306C, as well as a silent mutation to destroy the PAM site (p.I304=). (B–C) Transcript (B) and protein (C) expression levels did not differ between genotypes ($p$ = 0.28 and 0.68 respectively, Kruskal-Wallis). Symbols represent samples from individual mice, line represents median and error bars represent 95% confidence interval. (D) A representative western blot of forebrain membrane proteins probed for $K_V2.1$ protein and GRP75 as a normalization control show no difference. *Kcnb1*$^{fs/fs}$ that results in truncated protein with absent epitope was used as a negative control.

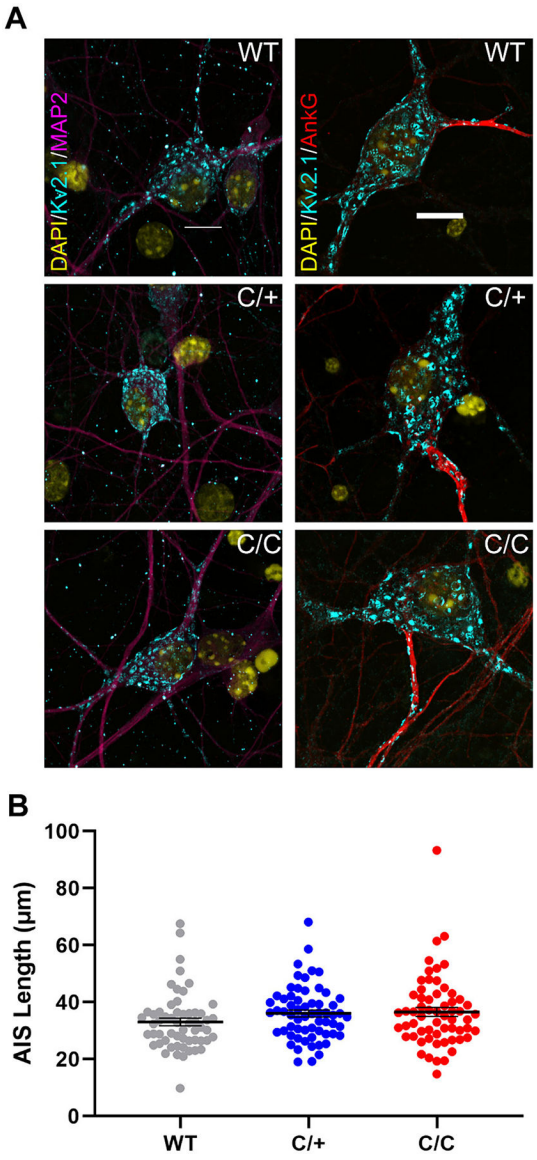


**Fig. 2.**

Subcellular localization $K_V2.1$ in cultured hippocampal neurons. (A) Cultured hippocampal neurons were immuno-labeled with $K_V2.1$ and neuronal processes (MAP2 for dendrites and AnkG for axon initial segment); 40× magnification for MAP2 and 60× for AnkG staining. (B) Length measurements of AIS were not different across different genotypes ($p = 0.1671$, one-way ANOVA; $n = 57–62$ per genotype).

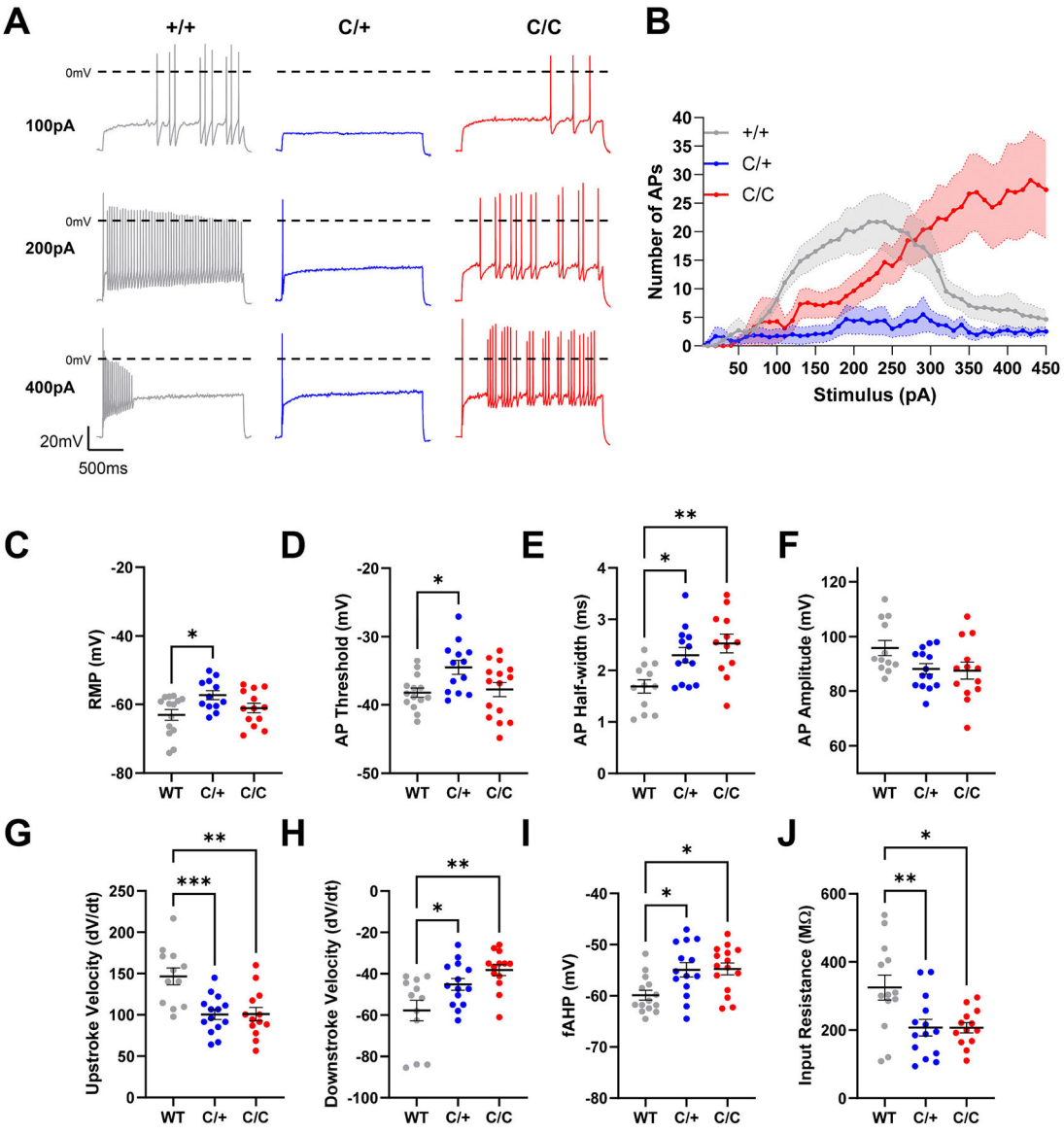


**Fig. 3.**

Hippocampal pyramidal neurons from *Kcnb1*$^{R306C}$ mice showed altered excitability (A) Representative action potential traces elicited by 100pA (top), 200pA (middle), and 400pA (bottom) current injections for WT (+/+), *Kcnb1*$^{C/+}$, and *Kcnb1*$^{C/C}$ neurons. (B) Input-output curves for WT (+/+), *Kcnb1*$^{C/+}$, and *Kcnb1*$^{C/C}$ neurons ($F(2, 1548) = 141.6$, $p < 0.0001$; Two-way ANOVA)(C) Resting membrane potential for WT, *Kcnb1*$^{C/+}$, and *Kcnb1*$^{C/C}$ neurons ($F(2, 36) = 4.0005$, $P = 0.0269$; One-way ANOVA; $^{*}p < 0.05$, Tukey's). (D) Action potential threshold for WT, *Kcnb1*$^{C/+}$, and *Kcnb1*$^{C/C}$ neurons ($F(2, 39) = 4.487$, $P = 0.0176$; One-way ANOVA; $^{*}p < 0.05$, Tukey's). (E) Action potential halfwidth for WT, *Kcnb1*$^{C/+}$, and *Kcnb1*$^{C/C}$ neurons ($F(2, 34) = 7.678$, $P = 0.0018$; One-way ANOVA; $^{*}p < 0.05$, $^{**}p < 0.01$, Tukey's). (F) Action potential amplitude for WT, *Kcnb1*$^{C/+}$, and *Kcnb1*$^{C/C}$ neurons($F(2, 36) = 3.115$, $P = 0.0565$; One-way ANOVA). (G) Upstroke velocity for WT, *Kcnb1*$^{C/+}$, and *Kcnb1*$^{C/C}$ neurons($F(2, 36) = 10.21$, $P = 0.0003$,; One-way ANOVA; $^{**}p <$

0.01, ***$p < 0.0001$, Tukey's). (H) Downstroke velocity for WT, *Kcnb1*$^{C/+}$, and *Kcnb1*$^{C/C}$ neurons ($F(2, 36) = 7.495$, $P = 0.0019$; One-way ANOVA; *$p < 0.05$, **$p < 0.01$, Tukey's). (I) Fast afterhyperpolarization for WT, *Kcnb1*$^{C/+}$, and *Kcnb1*$^{C/C}$ neurons($F(2, 40) = 5.976$, $P = 0.0054$; One-way ANOVA; *$p < 0.05$, Tukey's). (J) Input resistance for WT, *Kcnb1*$^{C/+}$, and *Kcnb1*$^{C/C}$ neurons ($F(2, 27) = 6.392$, $P = 0.0041$; One-way ANOVA; *$p < 0.05$, **$p < 0.01$, Tukey's).

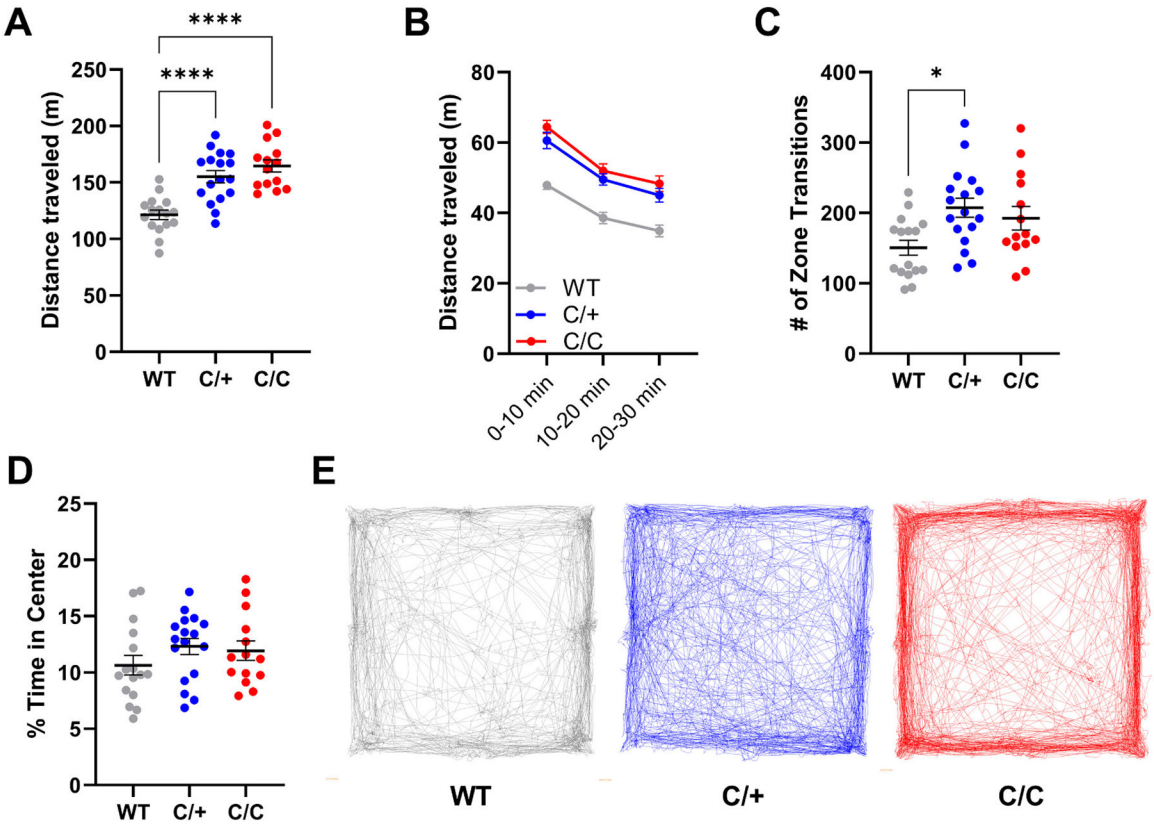


**Fig. 4.**

*Kcnb1*$^{R306C}$ mice have elevated exploratory locomotion in open field assay. (A) Total distance traveled in 30 min was affected by genotype ($F(2,44) = 20.6$, $p < 0.0001$; one-way ANOVA; ****$p < 0.0001$, Tukey's). (B) Locomotion assessed in 10-min bins across the 30-min session. *Kcnb1*$^{C/+}$ and *Kcnb1*$^{C/C}$ mice had elevated distance at all time points compared to WT ($F(2,44) = 19.11$, $p < 0.0001$; Two-way repeated measures ANOVA, Genotype). All groups showed similar habituation, with locomotion slowing over time and no significant genotype-by-time interaction (see Table 3). (C) Total number of zone transitions was affected by genotype ($F(2,44) = 4.86$, $p < 0.02$; one-way ANOVA; *$p < 0.02$, Tukey's). (D) Time spent in the center of area was not affected by genotype ($F(2,44) = 1.201$, $p > 0.31$). (E) Representative examples of open field paths for WT, *Kcnb1*$^{C/+}$ and *Kcnb1*$^{C/C}$ mice. For A, C and D, symbols represent individual mice and horizontal lines represent mean. Symbols in B represent group means. Error bars represent SEM (A-D).

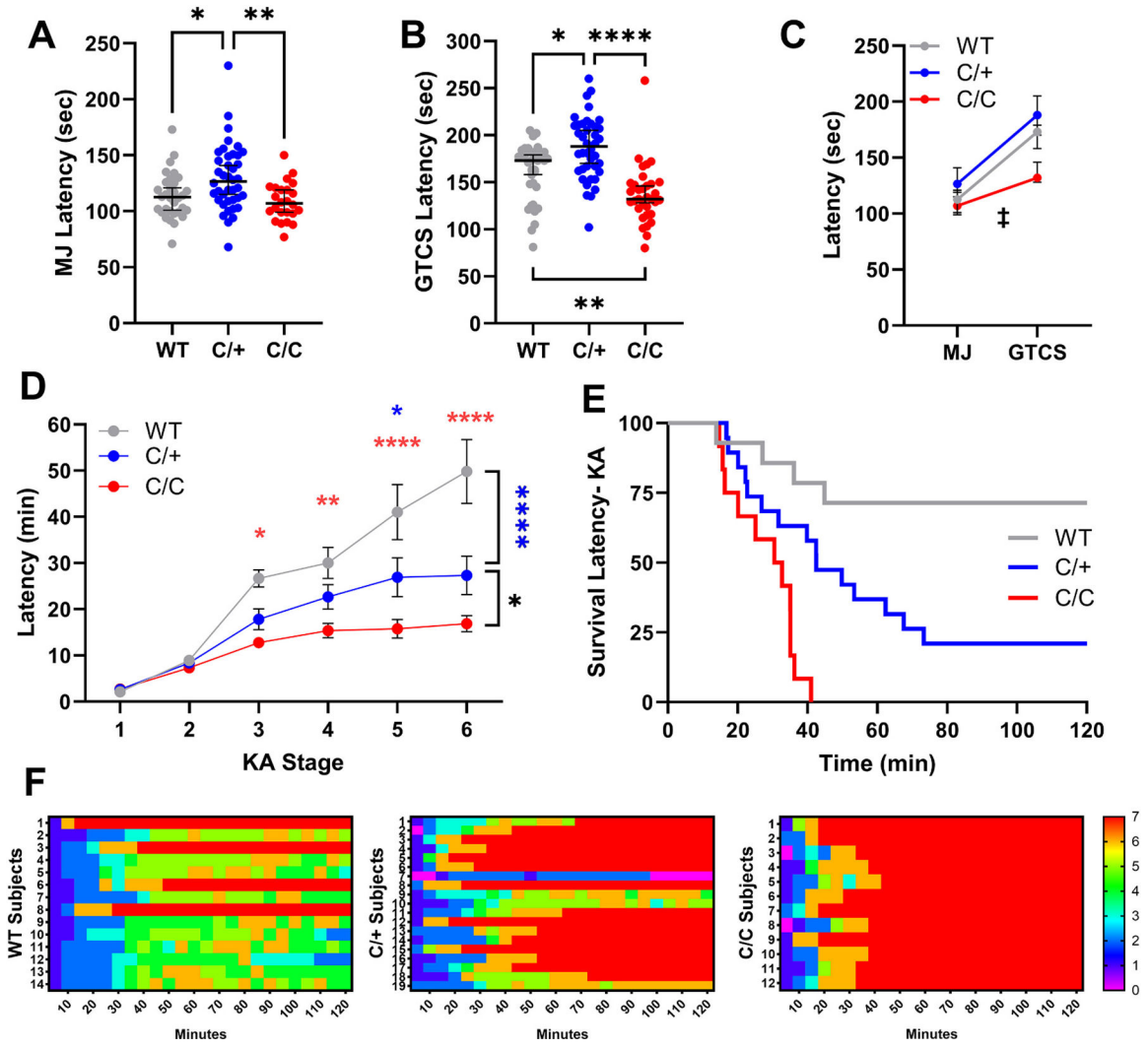


**Fig. 5.**

Altered susceptibility to seizures induced by chemoconvulsants in *Kcnb1*$^{C/+}$ and *Kcnb1*$^{C/C}$ mice. (A) Latency to the first flurothyl-induced MJ was affected by *Kcnb1* genotype (Kruskal-Wallis H(2) = 12.28, $p < 0.003$; *$p < 0.04$ and **$p < 0.004$, Dunn's). (B) Latency to flurothyl-induced GTCS was affected by *Kcnb1* genotype (Kruskal-Wallis H(2) = 35.83, $p < 0.0001$). *Kcnb1*$^{C/+}$ mice exhibited the longest median latency to GTCS, while *Kcnb1*$^{C/C}$ mice had the shortest latency to GTCS (*$p < 0.03$, **$p < 0.003$, ****$p < 0.0001$, Dunn's). For A-B, symbols represent individual mice, horizontal line represents median and error bars are 95% CI. (C) Progression from MJ to GTCS differed between genotypes (Kruskal-Wallis H(2) = 13.50, $p < 0.002$). *Kcnb1*$^{C/C}$ mice progressed the fastest between stages compared to WT (‡ $p < 0.005$) and *Kcnb1*$^{C/+}$ (‡ $p < 0.003$). (D) Progression of seizure stages scored on a modified Racine scale post KA administration. *Kcnb1*$^{C/C}$ mice progressed faster through stages 3–6 compared to WT and to stage 6 compared to *Kcnb1*$^{C/+}$ (WT v. *Kcnb1*$^{C/C}$ Red *$p < 0.02$ **$p < 0.008$, ****$p < 0.0001$; *Kcnb1*$^{C/+}$ v. *Kcnb1*$^{C/C}$ Black *$p < 0.03$). *Kcnb1*$^{C/+}$ mice progressed faster to stages 5 and 6 compared to WT (WT v. *Kcnb1*$^{C/+}$ Blue *$p < 0.02$, ****$p < 0.0001$). *P* values determined by Two-way ANOVA with Tukey's post-hoc tests

(see Table 3). Symbols represent the average latency of $n = 12–19$ mice per genotype. Error bars represent SEM. (E) Survival after KA administration was affected by *Kcnb1* genotype. 100% of $Kcnb1^{C/C}$ and 75% of $Kcnb1^{C/+}$ mice did not survive following KA administration, compared to 25% lethality in WT mice (LogRank Mantel-Cox $p < 0.0001$). (F) Heat map depicting individual level seizure severity post KA administration organized by genotype. Y axis represents individual mice and X axis represents 5 min bins.

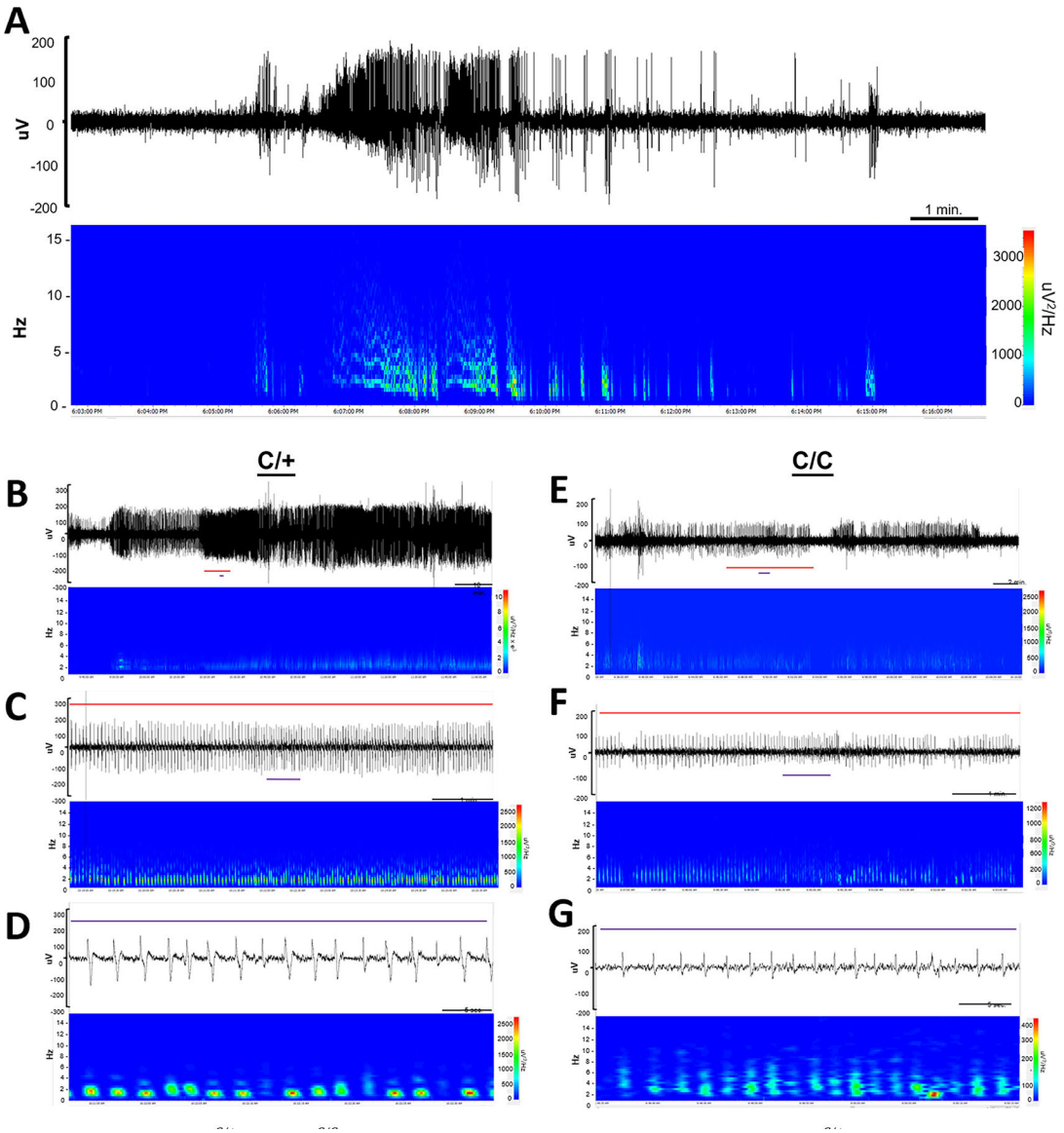


**Fig. 6.**

EEG abnormalities in *Kcnb1*$^{C/+}$ and *Kcnb1*$^{C/C}$ mice. (A) EEG trace of the single GTC seizure identified in a *Kcnb1*$^{C/+}$ mouse with corresponding spectral density array. Corresponding with the electrographic seizure, the *Kcnb1*$^{C/+}$ mouse displayed head bobbing and facial automatisms. All observable behaviors concluded when the baseline EEG activity returned to normal. One additional GTCS was detected in a *Kcnb1*$^{C/C}$ mouse with similar electrographic and behavioral manifestations. (B–D) Top trace represents a two-hour segment of continuous spike-wave discharges identified in a *Kcnb1*$^{C/+}$ mouse with corresponding spectral density array (B). Red line represents a ~ 7-min segment expanded in panel C and the purple line represents a ~ 40 s segment expanded in panel D. (E–G) Top trace represents a ~ 30-min segment of continuous spike-wave discharges identified in a *Kcnb1*$^{C/C}$ mouse with corresponding spectral density array (E). Red line represents a ~ 7-min trace expanded in panel F and purple line represents a ~ 40 s expanded in panel G.

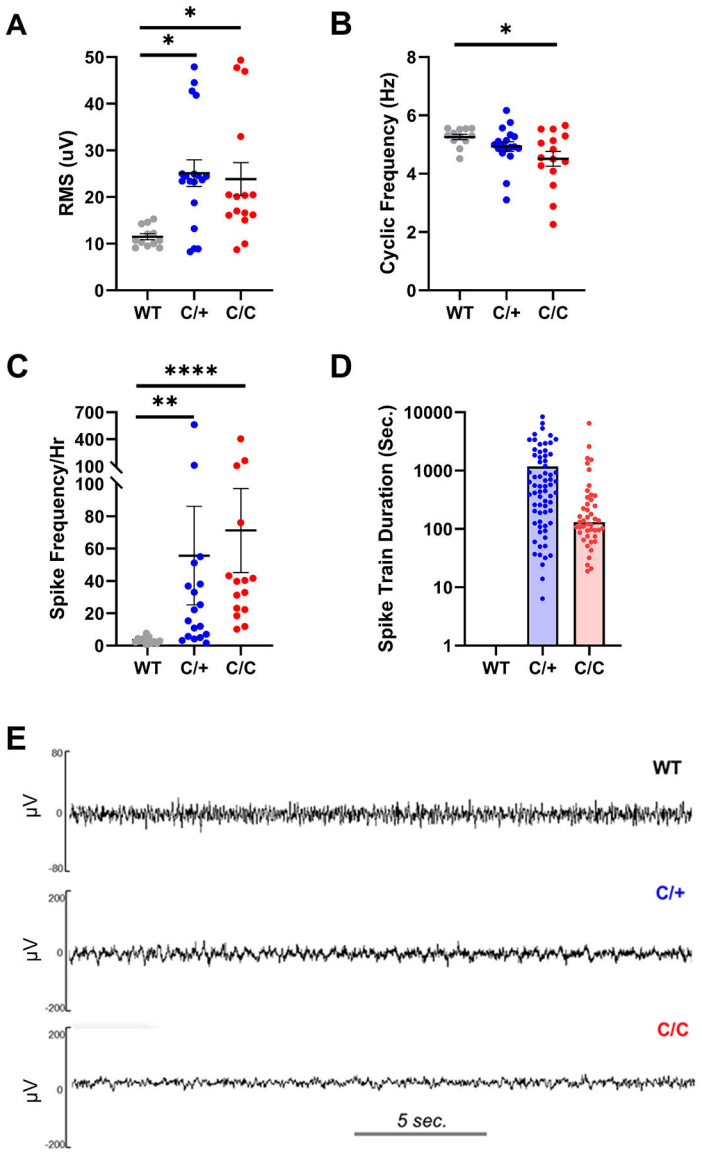


**Fig. 7.**

Slow, synchronous interictal activity and spike-wave discharge quantification for *Kcnb1*$^{C/+}$ and *Kcnb1*$^{C/C}$ mice. (A) Root square mean (RMS) was calculated to assess overall EEG amplitude. WT mice had an average RMS of 11.5 ± 0.64 μV, while *Kcnb1*$^{C/+}$ and *Kcnb1*$^{C/C}$ mice averaged 25.1 ± 2.9 μV and 23.9 ± 3.5 μV, respectively. *$p < 0.02$ Two-way ANOVA with Tukey's. (B) Cyclic frequency was calculated to determine periodic waveforms. WT mice had an average frequency of 5.3 ± 0.1 Hz, while *Kcnb1*$^{C/+}$ and *Kcnb1*$^{C/C}$ mice averaged 4.9 ± 0.7 Hz and 4.5 ± 0.3 Hz, respectively. **$p < 0.0003$, ****$p < 0.0001$ Two-way ANOVA with Tukey's. (C) 1–2.5 Hz SWDs were quantified. WT mice had an SWD frequency of 3.3 ± 0.6/h, while *Kcnb1*$^{C/+}$ and *Kcnb1*$^{C/C}$ mice averaged 55.6 ± 30.5/h and 71.2 ± 26.1/h, respectively. *$p < 0.02$ One-way ANOVA with Dunn's. (D) Spike train durations were quantified from manual review of EEG records. Four *Kcnb1*$^{C/+}$ (66%) and 3 *Kcnb1*$^{C/C}$ (60%) mice exhibited recurrent spike trains of various durations, while never

detected in WT EEG traces. Bars represent median length of spike trains. Symbols represent durations of individual trains. (E) Representative EEG traces from WT, *Kcnb1*$^{C/+}$ and *Kcnb1*$^{C/C}$ mice to illustrate the differences identified in RMS values and cyclic, synchronous activity. *Kcnb1*$^{C/+}$ and *Kcnb1*$^{C/C}$ mice consistently exhibited slowed background activity compared to WT littermates. Gray scale bar represents a 5 s period. A-C were quantified from 6-h epochs, on 3 separate days, per mouse. $n$ = 4–6 mice/genotype. Symbols represent individual 6-h epochs, line represents mean and error bars SEM. D was quantified from 70.1 to 119.6 h per mouse. $n$ = 4–6 mice/genotype.

**Table 1**

List of primers.

| Assay | Description | Sequence |
|---|---|---|
| Founder screening PCR | *Kcnb1* Primer 1 | 5'-TTGTCCTCTCCACCATTGCC |
| | *Kcnb1* Primer 2 | 5'-AGTCTTAGGGTAGATGTCTCCGT |
| RFLP genotyping (BsmI digest) | *Kcnb1* Primer 3 | 5'-TTGTGTGAGAGCCATGCTGT |
| | *Kcnb1* Primer 2 | 5'-AGTCTTAGGGTAGATGTCTCCGT |

**Table 2**

List of antibodies.

| Antibody | Immunogen | Manufacturer information | Concentration/Dilution used | RRID |
|---|---|---|---|---|
| K89/34 ($K_V$2.1) | Synthetic peptide aa 837–853 of rat $K_V$2.1 | NeuroMab; mouse IgG1 monoclonal | 2 μg/mL (WB) 1:1000 (ICC) | AB_10673392 |
| N52A/42 (GRP75/mortalin) | Identified as off-target mAb in screen for anti-SALM2 mAbs | NeuroMab; Mouse IgG1 mAb | 1 μg/mL (WB) | AB_2120479 |
| ab32454 (Map2) | Synthetic peptide within Rat MAP2 aa 1–100 (N terminal) | Abcam; rabbit polyclonal | 1:1000 (ICC) | AB_776174 |
| 386,003 (Ankyrin G) | Recombinant protein corresponding to AA 1784 to 1961 from mouse AnkyrinG | Synaptic Systems; rabbit polyclonal | 1:2000 (ICC) | AB_2661876 |
| 111-655-146 (Mouse IgG) | Mouse IgG | Jackson ImmunoResearch; goat anti-mouse IgG (H + L) cross-adsorbed secondary antibody, conjugated with Alexa Fluor 790 | 1:20,000 (WB) | AB_2338944 |
| A-21121 (Mouse IgG) | Mouse IgG1 | Thermo Fisher; goat anti-mouse IgG1 cross-adsorbed secondary antibody, conjugated with Alexa Fluor 488 | 1:2000 (ICC) | AB_2535764 |
| A-21245 (Rabbit IgG) | Rabbit IgG | Thermo Fisher; goat anti-rabbit IgG (H + L) highly cross-adsorbed secondary antibody, conjugated with Alexa Fluor 647 | 1:2000 (ICC) | AB_2535813 |

WB, western blot; ICC, immunocytochemistry.

## Table 3

Summary of statistical comparisons.

| Figure | Comparison | Test | Value | Post-hoc |
|---|---|---|---|---|
| 1b | Transcript | Kruskal-Wallis | $P = 0.2827$ | n/a |
| 1c | Protein | Kruskal-Wallis | $P = 0.6821$ | n/a |
| 2b | AIS length | One-way ANOVA | $F(2,177) = 1.807$, $P = 0.1671$ | n/a |
| 3b | Evoked neuronal excitability | Two-way ANOVA | $F(2, 1548) = 141.6$, $p < 0.0001$ | Tukey's |
| 3c | Resting membrane potential | One-way ANOVA | $F(2, 36) = 4.0005$, $P = 0.0269$ | Tukey's |
| 3d | AP threshold | One-way ANOVA | $F(2, 39) = 4.487$, $P = 0.0176$ | Tukey's |
| 3e | AP half-width | One-way ANOVA | $F(2, 34) = 7.678$, $P = 0.0018$ | Tukey's |
| 3f | AP Amplitude | One-way ANOVA | $F(2, 36) = 3.115$, $P = 0.0565$ | Tukey's |
| 3g | Upstroke velocity | One-way ANOVA | $F(2, 36) = 10.21$, $P = 0.0003$ | Tukey's |
| 3h | Downstroke velocity | One-way ANOVA | $F(2, 36) = 7.495$, $P = 0.0019$ | Tukey's |
| 3i | fAHP | One-way ANOVA | $F(2, 40) = 5.976$, $P = 0.0054$ | Tukey's |
| 3j | Input resistance | One-way ANOVA | $F(2, 27) = 6.392$, $P = 0.0041$ | Tukey's |
| 4a | Open field total distance | One-way ANOVA | $F(2,44) = 20.60$, $p < 0.0001$ | Tukey's |
| 4b | Open field 10-min bins | Two-way repeated measures ANOVA | $F(2,44) = 19.11$, $p < 0.0001$, Genotype; $F(3.821,168.1) = 119.0$, $p < 0.0001$, Time; $F(10,220) = 0.6897$, $P = 0.7336$, Interaction | Tukey's |
| 4c | Open field zone transitions | One-way ANOVA | $F(2,44) = 4.86$, $P = 0.012$ | Tukey's |
| 4d | Open field-center time | One-way ANOVA | $F(2,44) = 1.20$, $P = 0.31$ | n/a |
| 5a | Flurothyl - MJ latency | Kruskal-Wallis | $H(2) = 12.28$, $P = 0.0022$ | Dunn's |
| 5b | Flurothyl - GTCS latency | Kruskal-Wallis | $H(2) = 35.83$, $p < 0.0001$ | Dunn's |
| 5c | Flurothyl – MJ-GTCS interval | Kruskal-Wallis | $H(2) = 13.50$, $P = 0.0012$ | Dunn's |
| 5d | KA latency | Two-way repeated measures ANOVA | $F(5,209) = 31.48$, $p < 0.0001$, Genotype; $F(5, 209) = 44.12$, $p < 0.0001$, Racine Score; $F(10, 209) = 4.921$, $p < 0.0001$, Interaction | Tukey's |
| 5e | KA-survival | Mantel-Cox | $p < 0.0001$ | n/a |
| 7a | RMS | Two-way ANOVA | $F(2,37) = 5.322$, $P = 0.0093$ | Tukey's |
| 7b | Cyclic frequency | Two-way ANOVA | $F(2,37) = 3.548$, $P = 0.0389$ | Tukey's |
| 7c | Spike frequency | Kruskal-Wallis ANOVA | $p < 0.0001$ | Dunn's |

n/a = not applicable.

**Table 4**

EEG abnormalities in *Kcnb1*$^{R306C}$ mice.

| Genotype | Total hours *(manually reviewed)* | Select hours *(spike counting)* | *Spike calculations. n = 3 sets of 6 h/mouse* | | |
|---|---|---|---|---|---|
| | | | Avg. RMS (uv) ± SD | Avg. cyclic frequency (Hz) ± SD | Avg. spike frequency ($Hr^{-1}$) ± SD |
| WT | 117.4 | 18.0 | 9.5 ± 0.7 | 5.5 ± 0.1 | 3.4 ± 0.8 |
| | 119.6 | 18.0 | 10.5 ± 1.4 | 5.0 ± 0.5 | 2.2 ± 1.9 |
| | 70.1 | 18.0 | 14.7 ± 0.5 | 5.2 ± 0.1 | 2.6 ± 1.2 |
| | 70.2 | 18.0 | 11.2 ± 0.9 | 5.4 ± 0.1 | 5.1 ± 2.8 |
| | 70.3 | 18.0 | 24.8 ± 0.2 | 4.9 ± 0.02 | 3.5 ± 2.0 |
| | 73.3 | 18.0 | 45.0 ± 2.6 | 4.5 ± 1.3 | 222.9 ± 294.2 |
| | 72.2 | 18.0 | 18.5 ± 5.1 | 5.6 ± 0.6 | 17.5 ± 14.5 |
| C/+ | 70.4 | 18.0 | 8.7 ± 0.4 | 5.3 ± 0.1 | 8.0 ± 3.6 |
| | 70.6 | 18.0 | 23.7 ± 0.6 | 4.8 ± 0.2 | 19.4 ± 7.6 |
| | 70.4 | 18.0 | 30.0 ± 10.2 | 4.6 ± 0.8 | 62.4 ± 43.4 |
| | 73.4 | 18.0 | 11.9 ± 4.5 | 4.6 ± 0.3 | 13.5 ± 4.4 |
| | 70.6 | 18.0 | 17.7 ± 2.3 | 4.5 ± 0.5 | 214.8 ± 170.3 |
| | 70.3 | 18.0 | 26.1 ± 18.1 | 4.2 ± 1.7 | 28.4 ± 9.8 |
| C/C | 76.2 | 18.0 | 20.4 ± 0.2 | 5.6 ± 0.1 | 37.7 ± 5.7 |
| | 72.3 | 18.0 | 43.4 ± 9.0 | 3.6 ± 0.8 | 61.3 ± 40.7 |